Dynamic Systems and Applications 34 (2025) 61-81

COMPLEX DYNAMICS IN A LINEARLY DAMPED MORSE OSCILLATOR WITH MULTIPLE EXCITATIONS

S. SIVA SAKTHI PITCHAMMAL[1], S.M. ABDUL KADER[1], A. PONCHITRA[1], A. ZEENATH BAZEERA[1],V. CHINNATHAMBI[1,*]

[1]Department of Physics, Sadakathullah Appa College, Tirunelveli-627 011, Tamilnadu, India.(Affiliated to Manonmaniam Sundaranar University, Tirunelveli-12, Tamil Nadu, India.)

[*]Corresponding author: veerchinnathambi@gmail.com

ABSTRACT. In this paper, we examine the complex dynamics of a linearly damped Morse oscillator subjected under parametric and external excitations. The inclusion of a parametric excitation term adds complexity and interest to the analysis of the Morse oscillator. The unperturbed Morse oscillator features a degenerate fixed point at infinity, which is resolved by applying a McGehee-type transformation. This transformation regularizes the stationary fixed point, making it possible to apply the Melnikov method effectively to the system. Using analytical techniques, including the Melnikov theory, we derive threshold conditions for the occurrence of horseshoe chaos in the perturbed Morse oscillator. From these threshold conditions, we analyze the onset of horseshoe chaos numerically by measuring the time, τ_M, between successive changes in the sign of $M(\tau)$. Results show that as the depth of the potential well (a) increases, the threshold for horseshoe chaos also increases when varying the amplitude (f) of the external excitation. Conversely, the threshold for horseshoe chaos decreases as the amplitude (η) of the parametric excitation increases. The analytical findings are illustrated through numerical simulations, employing nonlinear analysis tools such as bifurcation diagrams, phase portraits, Poincaré maps, and measuring the time τ_M between successive sign changes in $M(\tau)$.

AMS (MOS) Subject Classification. 34C37, 34D10, 37C29, 37D45, 37J20, 65P20.

Key Words and Phrases. Perturbed Morse oscillator, Horseshoe chaos, Melnikov method, Parametric excitation, Chaos

1. INTRODUCTION

A vibrating system may be either forced or unforced, with forced systems playing a critical role in a wide range of applications across engineering and physics. The forces applied to such systems can be external, parametric, or a combination of both.

Received December 11, 2024 ISSN 1056-2176(Print); ISSN 2693-5295 (online)
www.dynamicpublishers.org https://doi.org/10.46719/dsa2023.32.03

For example, a spring-mass system subjected to a continuous sinusoidal force represents an externally forced system, where key parameters include the stiffness of the spring and the mass. Conversely, when the stiffness of the spring varies periodically over time, the system is considered parametrically forced. Parametric forcing arises naturally in many real-world scenarios. A classic example is a child on a swing who adjusts the position of their legs to inject energy into the system, thereby increasing the swing's amplitude. Other examples include a gear-pair system with periodically varying stiffness and a pendulum subjected to vertical oscillations [1-5]. Over the past two decades, there has been growing interest in research on nonlinear dynamics involving both parametric and external excitations [6-11].

The chaotic dynamics in nonlinear systems have long been a significant area of research, as such systems exhibit sensitivity to initial conditions and complex, unpredictable behaviors. Among the various forms of chaos, horseshoe dynamics present a particularly intriguing case. First introduced by Smale in the context of hyperbolic systems, horseshoe chaos involves phase space trajectories that undergo stretching and folding, creating a structure reminiscent of a horseshoe shape. This form of chaos is highly sensitive to perturbations, leading to intricate structures in the phase space of dynamical systems. Chaos is a well-established phenomenon in Hamiltonian dynamics. To analyze chaotic motion in perturbed nonlinear dynamical systems or identify the parameter regions where chaos occurs, the Melnikov technique serves as a highly effective tool. This method provides an analytic criterion for chaos in weakly perturbed Hamiltonian systems . The Melnikov function quantifies the transverse distance between the stable and unstable manifolds associated with an unstable periodic orbit. The presence of isolated odd zeros in the Melnikov function indicates transverse intersections of these manifolds, marking the onset of chaos. Inspired by Melnikov's seminal work [12], this approach was further developed in detail in [6,7] and is also discussed in [13]. This is the methodology we will employ here. Recently, the Melnikov method has been successfully applied to certain nonlinear systems to predict the occurrence of horseshoe chaos [14-24].

The Morse oscillator is one of the most prominent examples of an anharmonic oscillator and has found widespread applications. It serves as a realistic model for describing the vibrations of a diatomic molecule and is of significant interest both experimentally and theoretically. Additionally, the Morse oscillator remains a valuable model for the true interatomic potential energy. Numerous studies have explored the Morse oscillator using classical, semiclassical, and quantum mechanical methods [25-33]. Specifically, Guruparan et al. [34-36] analyzed various nonlinear phenomena in the classical Morse oscillator, including the coexistence of multiple attractors, hysteresis, and vibrational resonance under the influence of different periodic forces. Abirami et al. [37] discovered vibrational resonance in the Morse oscillator when subjected to two periodic forces. Knob et al. [38] studied the bifurcation structure of the classical Morse oscillator driven by periodic excitation, while Jing et al. [39] examined the bifurcations of periodic orbits leading to chaos in a damped and driven Morse oscillator. Additionally, the dynamics of a quasi-periodically forced Morse oscillator were investigated by Beigie et al. [40]. The parameter stability problem in parametrically excited systems is both important and challenging. However, the study of global bifurcations and chaotic dynamics in such systems is relatively less explored, particularly in the context of vibrations of a diatomic molecule with a time-varying damping coefficient and external excitation. In this paper, we analyze, both analytically and numerically, the effects of parametric and external periodic forcing on the dynamics of the Morse oscillator.

2. Damped and Parametrically Driven Morse Oscillator

The differential equation that describes the damped and driven Morse oscillator (DDMO) system is as follows:

$$\ddot{x} + \alpha\dot{x} - 2ab\, e^{-bx}(e^{-bx} - 1) = f \sin \omega t, \tag{2.1}$$

where x represents the distance between the atoms, $a > 0$ is the depth of the potential well (defined relative to the dissociated atoms), and $b > 0$ controls the width of the potential well (b small corresponds to a wide well, while large b corresponds to a narrow well). Here, α is the damping coefficient, and f and ω represent the amplitude and frequency of the driving force, respectively. Figure 1(a) shows the harmonic oscillator potential. A simple harmonic oscillator does not predict bond dissociation. It provides a good fit at low excitation but performs poorly at high excitation, explaining only the fundamental vibrations and not the overtones. In contrast, the Morse potential offers a better approximation for the potential energy of vibrating diatomic molecules. We now consider the Morse potential, a convenient model for interatomic interactions in diatomic molecules. The potential is given by [41]:

$$V(x) = a\,(e^{-2bx} - 2\, e^{-bx}). \tag{2.2}$$

Figure 1(b) illustrates the nature of the Morse potential curve for three different values of $a = 1.0$, 2.0, and 4.0. This curve demonstrates how real molecules do not exactly follow the law of simple harmonic motion. While real bonds are elastic, they do not adhere to Hooke's law due to inhomogeneities. The potential $V(x)$ has a local minimum at $x = 0$, with $V(x) \to \infty$ as $x \to -\infty$, and it approaches zero as $x \to \infty$. In the present work, we consider a periodic excitation of the parameter a is of the form is

$$a \longrightarrow a(1 + \eta \sin(\Omega t))$$

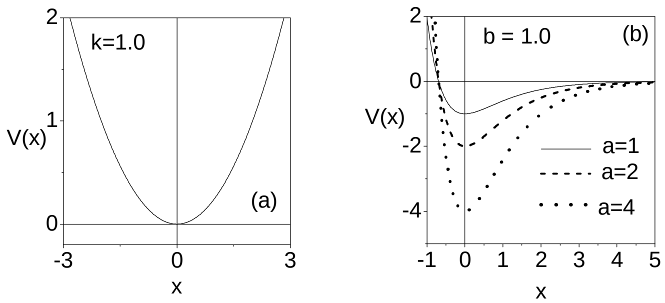

FIGURE 1. (a) Simple harmonic oscillator potential $V(x) = \frac{1}{2}kx^2$. (b) Morse potential curves for three different values of a.

where η and Ω represent the amplitude and frequency of the parametric periodic forcing, respectively. The perturbation is primarily due to small damping, along with parametric and external periodic excitations applied to the system. We focus on a Morse oscillator subjected to both parametric and external periodic excitations with two frequencies. The equation of motion for this combined excitation is given by:

$$\text{(2.3a)} \quad \dot{x} = y,$$

$$\text{(2.3b)} \quad \dot{y} = 2ab\, e^{-bx}(e^{-bx} - 1) + \epsilon\left[-\alpha y + 2ab\eta\, e^{-bx}(e^{-bx} - 1)\ \sin(\Omega t) + f\sin(\omega t)\right]$$

with $\epsilon << 1$. The unperturbed system is Hamiltonian, and the Hamiltonian function is given by

$$H(x, y) = \frac{y^2}{2} + 2a\, e^{-bx}(1 - \frac{1}{2}e^{-bx}) = I \tag{2.4}$$

From the Hamiltonian $H(x, y)$, we see that $y = \pm\sqrt{2I - 2ae^{-bx}(2 - e^{-bx})}$. Analyzing the unperturbed system, we identify the equilibrium point at $(\infty, 0)$, which is a non-hyperbolic equilibrium point. The phase portrait of the unperturbed system for various values of the potential well depth a (with $b = 1$) is shown in Fig. 2(a). The homoclinic orbits for various energy values I of the unperturbed system (with $a = 1$ and $b = 1$) are shown in Fig. 2(b). The homoclinic orbit occurs at $I = 0$.

Consider the unperturbed system,

$$\text{(2.5a)} \quad \dot{x_0} = y_0 = P(x, y)$$

$$\text{(2.5b)} \quad \dot{y_0} = 2ab\, e^{-bx}(e^{-bx} - 1) = Q(x.y)$$

The matrix

$$M = \begin{pmatrix} a_1 & a_2 \\ a_3 & a_4 \end{pmatrix}$$

where $a_1 = \frac{\partial P}{\partial x}|_{(x_0,y_0)}$, $a_2 = \frac{\partial P}{\partial y}|_{(x_0,y_0)}$, $a_3 = \frac{\partial Q}{\partial x}|_{(x_0,y_0)}$ and $a_4 = \frac{\partial Q}{\partial y}|_{(x_0,y_0)}$. Now we calculate the values of $a_1 = 0, a_2 = 1, a_3 = 2ab^2e^{-bx_0}[1-2e^{-bx_0}]$ and $a_4 = 0$. Therefore,

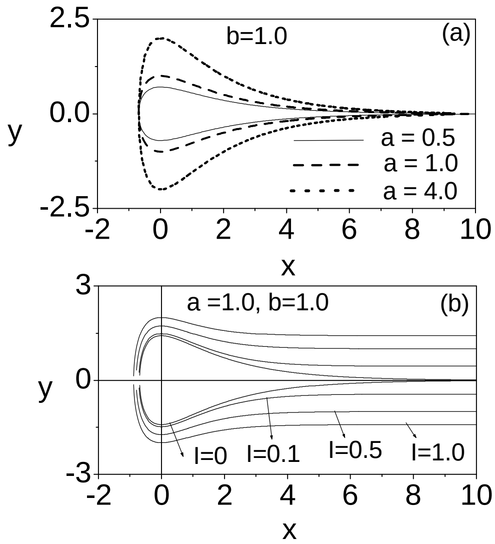

FIGURE 2. (a) Phase portrait of the unperturbed system for various values of depth of the potential well a with $b = 1$. (b) The homoclinic orbits for various energy values I of the unperturbed system with $a = 1$ and $b = 1$. The homoclinic orbit occurs for $I = 0$.

the matrix M becomes,

$$M = \begin{pmatrix} 0 & 1 \\ 2ab^2e^{-bx_0}[1 - 2e^{-bx_0}] & 0 \end{pmatrix}$$

and $det(M) = -2ab^2e^{-bx_0}[1 - 2e^{-bx_0}]$. det(M) $= 0$ at $x_0 = \infty$. Also the system (Eq.2.3) has the fixed point $(x^*, y^*) = (\infty, 0)$. For the fixed point $(\infty, 0)$, the determinant of the Jacobian is zero, indicating that both eigenvalues of the equilibrium point $(\infty, 0)$ are zero. Therefore, this point is a degenerate fixed point, and the Melnikov method cannot be directly applied. A McGehee-type transformation resolves the degeneracy of the stationary point at infinity, with the parabolic orbit of the original system corresponding to a homoclinic orbit in the new coordinates. Consequently, the Melnikov method becomes applicable, revealing a chaotic region in the phase space near the parabolic orbit of the unperturbed system.

3. McGehee-type coordinate transformation and Melnikov analysis

3.1. **McGehee-type coordinate transformation.** : To desigularize the equilibrium point $(\infty, 0)$, we perform the following McGehee-type transformation [42,43,44] This transformation changes the variables to local coordinates at ∞ and reparametrizes the time

$$x = -\frac{2}{b}\, ln(u), \tag{3.1a}$$

$$y = v \tag{3.1b}$$

$$\frac{ds}{dt} = \frac{-b}{2}u, \quad \Rightarrow t(s) = -\frac{2}{b}\int \frac{ds}{u(s)} \tag{3.1c}$$

In new coordinates, the (Eq.2.3) are given by

$$\dot{x} = y \tag{3.2a}$$

$$\frac{du}{ds} = y = v. \tag{3.2b}$$

Since, $x = -\frac{2}{b}ln(u) \Longrightarrow ln(u) = -\frac{bx}{2}, \quad u = e^{-bx/2} \Longrightarrow u^2 = e^{-bx}$

$$\dot{y} = \frac{dv}{ds} = 2abu^2[u^2-1] + \epsilon\left[-\alpha v + 2ab\, u^2(u^2-1)\,\eta\sin(\Omega t) + f\sin(\omega t)\right] \tag{3.2c}$$

Since, $b = -\frac{2}{u}\frac{ds}{dt}$

$$\begin{aligned}
\frac{dv}{ds} &= 2a\left[-\frac{2}{u}\frac{ds}{dt}\right]u^2(u^2-1) + \epsilon\left[-\alpha v + 2a\left[-\frac{2}{u}\frac{ds}{dt}\right]u^2(u^2-1)\eta\sin(\Omega t) + f\sin(\omega t)\right]\\
&= -4au(u^2-1)\frac{ds}{dt} + \epsilon\left[-\alpha v - 4au(u^2-1)\frac{ds}{dt}\eta\sin(\Omega t) + f\sin(\omega t)\right]\\
&= 4au(1-u^2)\frac{ds}{dt} + \epsilon\left[-\alpha v + 4au(1-u^2)\frac{ds}{dt}\eta\sin(\Omega t) + f\sin(\omega t)\right]
\end{aligned} \tag{3.3}$$

Since $-\alpha v = -\alpha y$

$$\begin{aligned}
\frac{dv}{ds} &= 4au(1-u^2) + \epsilon\left[-\frac{\alpha v}{\frac{ds}{dt}} + 4au(1-u^2)\eta\sin(\Omega t(s)) + \frac{f}{\frac{ds}{dt}}\sin(\omega t(s))\right]\\
&= 4au(1-u^2) + \epsilon\left[-\frac{\alpha v}{(-bu/2)} + 4au(1-u^2)\eta\sin(\Omega t(s)) + \frac{f}{(-bu/2)}\sin(\omega t(s))\right]\\
\frac{dv}{ds} &= 4au(1-u^2) + \epsilon\left[\frac{2\alpha v}{(bu)} + 4au(1-u^2)\eta\sin(\Omega t(s)) - \frac{2f}{(bu)}\sin(\omega t(s))\right]
\end{aligned} \tag{3.4}$$

The corresponding unperturbed system is,

$$\frac{du_0}{ds} = v_0, \quad \frac{dv_0}{ds} = 4au_0(1-u_0^2) \tag{3.5}$$

In this case, the fixed point is $(u_0, v_0) = (0, 0)$ and is now a non-degenerate hyperbolic fixed point. Now the matrix

$$M = \begin{pmatrix} a_1 & a_2 \\ a_3 & a_4 \end{pmatrix} = \begin{pmatrix} 0 & 1 \\ 4a(1-3u_0^2) & 0 \end{pmatrix} \tag{3.6}$$

$$(3.7)\qquad det(M-\lambda I)=\begin{pmatrix} -\lambda & 1 \\ 4a(1-3u_0^2) & -\lambda \end{pmatrix} \Longrightarrow \lambda^2-4a(1-3u_0^2)=0.$$

Since $u_0 = 0$, $\lambda^2 - 4a = 0 \;\Rightarrow \lambda = \pm 2\sqrt{a}$. So the fixed point $(u_0, v_0) = (0, 0)$ is a non-degenerate hyperbolic fixed point with eigenvalues $\lambda_{1,2} = \pm 2\sqrt{a}$. The system is now suitable for applying the Melnikov method. Rewriting the Hamiltonian in the new coordinates gives the following first integral. ,

$$(3.8)\qquad I=\frac{1}{2}\,v_0^2+au_0^2(u_0^2-2).$$

We can express the first integral as $v_0 = \pm\sqrt{2I - 2au_0^2(u_0^2-2)}$. The homoclinic solution corresponds to $I = 0$. For $I \neq 0$, Homoclinic bifurcations occurs. The homoclinic solution corresponds to

$$(3.9a)\qquad u_0(s,s_0) \;=\; \pm\sqrt{2}\,\mathrm{sech}\left(2\sqrt{a}(s-s_0)\right),$$

$$(3.9b)\qquad v_0(s,s_0) \;=\; \mp 2\sqrt{2a}\,\mathrm{sech}\left(2\sqrt{a}(s-s_0)\right)\,\tanh\left(2\sqrt{a}(s-s_0)\right).$$

Using the new coordinates, the parameterized time becomes

$$\begin{aligned} t(s) &= -\frac{2}{b}\int\frac{ds}{u(s)}=-\frac{2}{b}\int\frac{ds}{\sqrt{2}\,\mathrm{sech}(2\sqrt{a}(s-s_0))} \\ &= \frac{-2}{\sqrt{2}b}\int\cosh(2\sqrt{a}(s-s_0))ds \\ &= \frac{-2}{\sqrt{2}b}\left[\sinh(2\sqrt{a}(s-s_0))\right](2\sqrt{a})^{-1}+\tau \\ (3.10)\qquad &= \frac{-1}{b\sqrt{2a}}\left[\sinh(2\sqrt{a}(s-s_0))\right]+\tau \end{aligned}$$

where τ is the constant of integration. Thus

$$(3.11a)\qquad t(s) \;=\; \tau-\frac{1}{b\sqrt{2a}}\left[\sinh(2\sqrt{a}(s-s_0))\right]$$

$$(3.11b)\qquad \Rightarrow\; t(s) \;=\; \tau-\frac{s'}{b\sqrt{2a}}$$

where $s' = \sinh\left(2\sqrt{a}(s-s_0)\right)$ and τ is the constant of integration which corresponds to initial time.

3.2. **Melnikov Analysis.** The application of Melnikov criterion allows of easy prediction of the critical values of parameters that make chaos suppression/appearance possible. The Melnikov function may be written in the form [43]

$$(3.12)\qquad M(\tau)=\int_{-\infty}^{\infty}\hat{X}_0^s I ds$$

$\hat{X}_0^s$ is the vector field of the perturbation.

$$(3.13)\qquad \hat{X}_0^s=\left[\frac{2\alpha v_0}{(bu_0)}+4au_0(1-u_0^2)\eta\sin(\Omega t(s,s_0))-\frac{2f}{bu_0}\sin(\omega t(s,s_0))\right]\frac{\partial}{\partial v_0}$$

which acts on the first integral (Eq.3.8). For the practical analysis of the Melnikov integral one needs the unperturbed separatrix solutions as a function of t and τ. Now $\frac{\partial I}{\partial v_0} = v_0$ and

$$\hat{X}_0^s = \left[\frac{2\alpha v_0}{(bu_0)} + 4au_0(1-u_0^2)\eta\sin(\Omega t(s,s_0)) - \frac{2f}{bu_0}\sin(\omega t(s,s_0))\right]\frac{\partial I}{\partial v_0} \tag{3.14}$$

$$\hat{X}_0^s = \left[\frac{2\alpha v_0}{(bu_0)} + 4au_0(1-u_0^2)\eta\sin(\Omega t(s,s_0)) - \frac{2f}{bu_0}\sin(\omega t(s,s_0))\right]v_0. \tag{3.15}$$

Then the Melnikov becomes

$$\begin{aligned} M(\tau) &= \int_{-\infty}^{\infty}\hat{X}_0^s I ds \\ &= \left[\frac{2\alpha v_0^2}{(bu_0)} + 4au_0v_0(1-u_0^2)\eta\sin(\Omega t(s,s_0)) - \frac{2f}{bu_0}v_0\sin(\omega t(s,s_0))\right]ds \qquad (3.16) \\ &= \quad M_1 \qquad\qquad + M_2 \qquad\qquad + \quad M_3 \end{aligned}$$

where

$$M_1 = \int_{-\infty}^{\infty}\left[\frac{2\alpha v_0^2}{(bu_0)}\right]ds \tag{3.17}$$

$$M_2 = \int_{-\infty}^{\infty} 4au_0v_0(1-u_0^2)\eta\sin(\Omega t(s,s_0))ds \tag{3.18}$$

$$M_3 = -\int_{-\infty}^{\infty}\frac{2f}{bu_0}v_0\sin(\omega t(s,s_0))ds \tag{3.19}$$

Now we calculate the integrals M_1, M_2 and M_3. First we calculate the integral value of M_1

$$\begin{aligned} M_1 &= \int_{-\infty}^{\infty}\left[\frac{2\alpha v_0^2}{(bu_0)}\right]ds \\ &= \int_{-\infty}^{\infty} 2\alpha\frac{\left[-2\sqrt{2a}\,\mathrm{sech}\,(2\sqrt{a}(s-s_0))\ \tanh\,(2\sqrt{a}(s-s_0))\right]^2}{b\,\sqrt{2}\,\mathrm{sech}\,(2\sqrt{a}(s-s_0))}ds \\ &= \frac{8\sqrt{2}a\alpha}{b}\int_{-\infty}^{\infty}\mathrm{sech}[2\sqrt{a}(s-s_0)]\tanh^2[2\sqrt{a}(s-s_0)]ds \end{aligned}$$

Since $u = 2\sqrt{a}(s-s_0)$, $\quad du = 2\sqrt{a}ds$, $\quad ds = \frac{du}{2\sqrt{a}}$

$$\begin{aligned} M_1 &= \frac{8\sqrt{2}a\alpha}{b}\int_{-\infty}^{\infty}\mathrm{sech}(u)\tanh^2(u)\frac{du}{2\sqrt{a}} \\ &= \frac{4\sqrt{2a}\alpha}{b}\int_{-\infty}^{\infty}\mathrm{sech}(u)\tanh^2(u)du \\ &= \frac{4\sqrt{2a}\alpha}{b}\times\frac{\pi}{2}. \end{aligned}$$

Therefor the value of integral M_1 is

$$M_1 = \frac{2\sqrt{2a}\alpha}{b}\,\pi \tag{3.20}$$

Next we workout the integral value of M_2

$$
\begin{aligned}
M_2 &= \int_{-\infty}^{\infty} 4au_0v_0(1-u_0^2)\eta\sin(\Omega t(s,s_0))ds \\
&= 4a\eta\int_{-\infty}^{\infty} u_0v_0(1-u_0^2)\sin(\Omega t(s,s_0))ds \\
&= 4a\eta\int_{-\infty}^{\infty}\left[\sqrt{2}\,\mathrm{sech}(2\sqrt{a}(s-s_0))\right]\left[-2\sqrt{2a}\,\mathrm{sech}(2\sqrt{a}(s-s_0))\tanh(2\sqrt{a}(s-s_0))\right] \\
&\quad \left[1-2\mathrm{sech}^2(2\sqrt{a}(s-s_0))\right]\ \sin(\Omega t(s,s_0))ds. \\
&= -8a\eta 2\sqrt{2a}\int_{-\infty}^{\infty}\mathrm{sech}^2(2\sqrt{a}(s-s_0))\tanh(2\sqrt{a}(s-s_0))\sin(\Omega t(s,s_0)) \\
&\quad +8a\eta 2\sqrt{2a}\int_{-\infty}^{\infty} 2\mathrm{sech}^4(2\sqrt{a}(s-s_0))\tanh(2\sqrt{a}(s-s_0))\sin(\Omega t(s,s_0))ds,
\end{aligned}
$$

Since $u=2\sqrt{a}(s-s_0)$, $\quad du=2\sqrt{a}ds$, $\quad ds=\frac{du}{2\sqrt{a}}$

$$
\begin{aligned}
M_2 &= -8a\eta\int_{-\infty}^{\infty}\mathrm{sech}^2 u\tanh u\ \sin(\Omega t)du + 8a\eta\ 2\int_{-\infty}^{\infty} 2\mathrm{sech}^4 u\tanh u\sin\Omega t du, \\
&= \qquad M_{21} \ + \qquad M_{22}.
\end{aligned}
$$

Since,

$$
\begin{aligned}
\sin\Omega t &= \sin\Omega(\tau-\frac{1}{b\sqrt{2a}}\sinh(2\sqrt{a}(s-s_0)) \\
&= \sin\Omega(\tau-\frac{s'}{b\sqrt{2a}}) \\
&= \sin\Omega\tau\cos\frac{\Omega s'}{b\sqrt{2a}} - \cos\Omega\tau\sin\frac{\Omega s'}{b\sqrt{2a}}
\end{aligned}
$$

Now substituting the above in the M_{21} and M_{22} equations and simplifying we get

$$
\begin{aligned}
M_{21} &= -8a\eta\int_{-\infty}^{\infty}\mathrm{sech}^2 u\tanh u\left[\sin\Omega\tau\cos\frac{\Omega s'}{b\sqrt{2a}} - \cos\Omega\tau\sin\frac{\Omega s'}{b\sqrt{2a}}\right]du \\
&= -8a\eta\int_{-\infty}^{\infty}\mathrm{sech}^2 u\tanh u\sin\Omega\tau\cos\frac{\Omega s'}{b\sqrt{2a}}du \\
&\quad +8a\eta\int_{-\infty}^{\infty}\mathrm{sech}^2 u\tanh u\cos\Omega\tau\sin\frac{\Omega s'}{b\sqrt{2a}}du
\end{aligned}
\tag{3.21}
$$

Similarly we can calculate the integral M_{22}

$$
\begin{aligned}
M_{22} &= 16a\eta\int_{-\infty}^{\infty}\mathrm{sech}^4 u\tanh u\sin\Omega\tau\cos\frac{\Omega s'}{b\sqrt{2a}}du \\
&\quad -16a\eta\int_{-\infty}^{\infty}\mathrm{sech}^4 u\tanh u\cos\Omega\tau\sin\frac{\Omega s'}{b\sqrt{2a}}du.
\end{aligned}
\tag{3.22}
$$

In Eqs.(3.21) and (3.22), the first part of the integral value is zero and the remaining integral value, that is,

$$\begin{aligned} M_{21} &= 8a\eta\cos\Omega\tau \int_{-\infty}^{\infty} \mathrm{sech}^2 u \tanh u \sin\frac{\Omega s'}{b\sqrt{2a}} du \\ M_{22} &= -16a\eta\cos\Omega\tau \int_{-\infty}^{\infty} \mathrm{sech}^4 u \tanh u \sin\frac{\Omega s'}{b\sqrt{2a}} du \\ M_2 &= M_{21} + M_{22} \end{aligned}$$

After integrating the integral value of M_2 is

$$M_2 = -\frac{\pi\sqrt{2a}\Omega\eta}{b}\left(\frac{\Omega}{b\sqrt{2a}} - 1\right) e^{\left(-\frac{\Omega}{b\sqrt{2a}}\right)} \cos\Omega\tau. \tag{3.23}$$

Then we calculate the integral value of M_3

$$\begin{aligned} M_3 &= -\int_{-\infty}^{\infty} \frac{2f}{bu_0} v_0 \sin(\omega t(s,s_0))ds \\ &= -\frac{2f}{b}\int_{-\infty}^{\infty} \frac{v_0}{u_0}\sin(\omega t(s,s_0))ds \end{aligned} \tag{3.24}$$

Before we compute the integral (Eq.3.24), we make the substitution,

$$s' = \sinh(2\sqrt{a}(s - s_0)) \tag{3.25}$$

After rewriting the integral (Eq.3.24) interms of s', it becomes,

$$M_3(s') = \frac{f}{b}\int_{-\infty}^{\infty} \frac{2s'}{(1+s'^2)} \sin\omega t(s')ds' \tag{3.26}$$

and

$$t(s') = \tau - \frac{s'}{b\sqrt{a}} \tag{3.27}$$

Note that

$$\begin{aligned} \sin\omega t &= \sin\omega(\tau - \frac{s'}{b\sqrt{2a}}) \\ &= \sin\omega\tau\cos\frac{\omega s'}{b\sqrt{2a}} - \cos\omega\tau\sin\frac{\omega s'}{b\sqrt{2a}} \end{aligned}$$

Therefore Eq.(3.26) becomes

$$M_3(\tau) = \frac{f}{b}\int_{-\infty}^{\infty} \frac{2s'}{(1+s'^2)}\left[\sin\omega\tau\cos\frac{\omega s'}{b\sqrt{2a}} - \cos\omega\tau\sin\frac{\omega s'}{b\sqrt{2a}}\right] ds' \tag{3.28}$$

Since

$$\int_{-\infty}^{\infty} \frac{s'}{1+s'^2}\cos\frac{\omega s'}{b\sqrt{2a}} ds' = 0 \tag{3.29}$$

and

$$\int_{-\infty}^{\infty} \frac{s'}{1+s'^2}\sin\frac{\omega s'}{b\sqrt{2a}} ds' = \pi e^{-\omega/b\sqrt{2a}} \tag{3.30}$$

Therefore Eq.(3.28) becomes

$$M_3(\tau) = \frac{2\pi f}{b}\, e^{-\omega/b\sqrt{2a}}\, \cos\omega\tau \tag{3.31}$$

Substituting the Eqs.(3.20),(3.23) and (3.31) in Eq.(3.16), we get

(3.32)

$$M^{\pm}(\tau) = \frac{2\sqrt{2a}\alpha}{b}\,\pi \mp \frac{\pi\sqrt{2a}\Omega\eta}{b}\left(\frac{\Omega}{b\sqrt{2a}} - 1\right) e^{\left(-\frac{\Omega}{b\sqrt{2a}}\right)} \cos\Omega\tau \pm \frac{2\pi f}{b}\, e^{-\omega/b\sqrt{2a}}\, \cos\omega\tau$$

Now the Eq.(3.32) can be written as

$$M^{\pm}(\tau) = A \pm B\eta\cos\Omega\tau \pm Cf\cos\omega\tau. \tag{3.33a}$$

where

$$A = \frac{2\sqrt{2a}\alpha}{b}\,\pi \tag{3.33b}$$

$$B = -\frac{\pi\sqrt{2a}\Omega}{b}\left(\frac{\Omega}{b\sqrt{2a}} - 1\right) e^{\left(-\frac{\Omega}{b\sqrt{2a}}\right)} \tag{3.33c}$$

$$C = \frac{2\pi}{b}\, e^{-\omega/b\sqrt{2a}}. \tag{3.33d}$$

From these equations (Eqs.3.33), we can obtain the necessary condition for the occurrence of horseshoe chaos.

4. **Results of Numerical simulations**

In this section, we study the occurrence of horseshoe chaos both analytically and numerically, focusing on the onset of chaos in the system described by Eq.(2.3) for two cases: $\omega = \Omega$ and $\omega \neq \Omega$. First, we analyze the occurrence of horseshoe chaos for the case $\omega = \Omega$ by varying the amplitude f of the external periodic force while keeping the value of η fixed. Then, we fix the value of f and vary the amplitude η of the parametric excitation force. Finally, we examine the case where $\omega \neq \Omega$.

4.1. **Horesshoe chaos for the case $\omega = \Omega$.**

4.1.1. **Horseshoe Chaos for Varying f and Fixed η.** We analyze the occurrence of horseshoe chaos numerically by measuring the time τ_M elapsed between two successive changes in the sign of $M(\tau)$. The value of τ_M can be determined from Eq. (3.33). In our numerical simulations, we fix the parameters in Eq. (3.33) as $\alpha = 0.8$, $b = 3.0$, and $\Omega = \omega = 2.0$. Figure 3 shows the variation of $1/\tau_M^{\pm}$ versus f for two values of a, namely $a = 0.5$ and $a = 1.0$. The continuous curve represents the inverse of the first intersection time $(1/\tau_M^{+})$ of the stable and unstable branches of the homoclinic orbits W^{+}, while the dashed curve corresponds to the orbits W^{-}. Horseshoe dynamics does not occur when $1/\tau$ is zero, but it occurs in the region where $1/\tau > 0$. In Fig. 3(a), where a is fixed at 0.5, $1/\tau_M^{+}$ is zero (i.e., $\tau_M^{\pm}$ is infinite) for $0 < f < 0.805414$, indicating that no horseshoe chaos occurs in this range of f. For values of f greater than

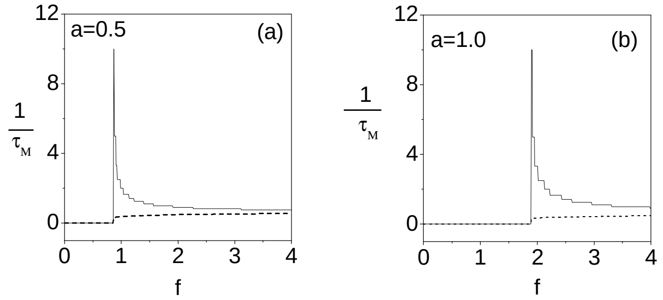

FIGURE 3. Variation of $1/\tau_M^{\pm}$ versus f for two values of $a = 0.5$ and 1.0. Continuous curve is for positive sign of $M(\tau)$ and dashed curve is for negative sign of $M(\tau)$ given by Eq.(3.33). The values of the other parameters in Eq.(3.33) are $\eta = 0.1, \alpha = 0.8, b = 3.0$, $\Omega = \omega = 2$.

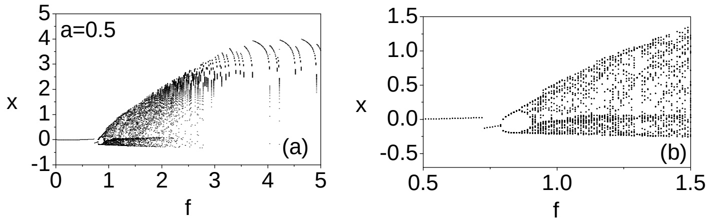

FIGURE 4. (a) Bifurcation diagram of the system (Eq.2.3) as a function of f for $a = 0.5$. (b) Magnification of a part of bifurcation diagram of Fig.4(a). The values of the other parameters in Eq.(2.3) are $\eta = 0.1, \alpha = 0.8, b = 3.0, \Omega = \omega = 2.0$.

0.805414, both $M^+(\tau)$ and $M^-(\tau)$ oscillate, and therefore $1/\tau_M^{\pm}$ is nonzero. Thus, when $f > 0.805414$, horseshoe chaos becomes possible. In Fig. 3(b), with a fixed at 1.0, $1/\tau_M^{\pm}$ is zero for $0 < f < 1.891458$, meaning no horseshoe chaos occurs in this interval. For $f > 1.891458$, $1/\tau_M^{\pm}$ becomes nonzero, indicating that horseshoe chaos is possible. Figure 3 illustrates that the Melnikov threshold for horseshoe chaos (f_M) increases as the depth of the potential well increases.

To verify the analytical results obtained above, we numerically integrated the system (Eq. 2.3) using the fourth-order Runge-Kutta method to investigate the homoclinic chaos in the system. First, we examine the effect of the external forcing term on the oscillator and how the dynamics of the oscillator are affected as the forcing amplitude f is varied. Figure 4(a) shows the bifurcation diagram of the system (Eq. 2.3) for $a = 0.5$, $\eta = 0.1$, $\alpha = 0.8$, $b = 3.0$, and $\Omega = \omega = 2.0$. For small values of f, the system has two coexisting periodic attractors with period $T(= 2\pi/\omega)$. One attractor is in the region $x < 0$, and the other is in the region $x > 0$. As f increases, the period-T attractor in the region $x < 0$ undergoes a period-doubling bifurcation, leading to the onset of chaos, which is clearly seen in Fig. 4(a). For clarity, a magnified part of the bifurcation diagram from Fig. 4(a) is shown in Fig. 4(b), where coexisting attractors, period-doubling bifurcations, and chaotic orbits are clearly visible. For

$a = 0.5$, the onset of chaos occurs at $f_c = 0.813723$. The bifurcation diagram of the system (Eq. 2.3) for $a = 1.0$ is shown in Fig. 5(a), where we again observe various bifurcations and chaotic orbits. For $a = 1.0$, the onset of chaos occurs at $f_c = 1.900893$. For clarity, a magnified part of the bifurcation diagram from Fig. 5(a) is shown in Fig. 5(b).

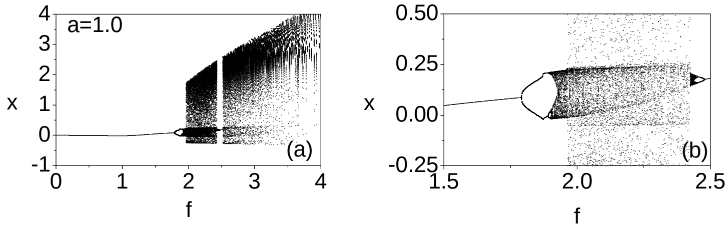

FIGURE 5. (a) Bifurcation diagram of the system (Eq.2.3) as a function of f for $a = 0.5$. (b) Magnification of a part of bifurcation diagram Fig.5(a). The values of the other parameters in Eq.(2.3) are $\eta = 0.1, \alpha = 0.8, b = 3.0, \Omega = \omega = 2.0$.

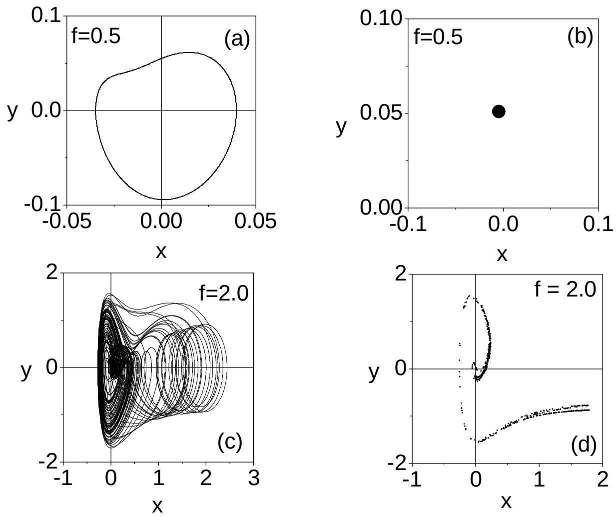

FIGURE 6. Phase portraits and the corresponding Poincaré maps of the system (Eq.2.3) for showing the (a-b) periodic orbit for $f = 0.5$ and (c-d) chaotic orbit for $f = 2.0$. The values of the other parameters in Eq.(2.3) are $\eta = 0.1, \alpha = 0.8, b = 3.0, \omega = \Omega = 2.0$.

Next, we check the threshold of the external forcing amplitude f for the onset of possible chaos, as obtained analytically. For $a = 0.5$, the onset of horseshoe chaos occurs at $f_M = 0.805414$ (Fig. 3(a)), while the onset of chaos is found at $f_c = 0.813723$ (Fig.4). Similarly, for $a = 1.0$, the onset of horseshoe chaos occurs at $f_M = 1.891458$ (Fig. 3(b)), while the onset of chaos occurs at $f_c = 1.900817$ (Fig.5). The numerical results agree well with the theoretical predictions. Furthermore, the analytical prediction is also verified by plotting the phase portrait and Poincaré map.

Figure 6 shows the phase portrait and the corresponding Poincaré map for two values of f, namely, $f = 0.5$ and $f = 2.0$, chosen from Fig. 3(b). For $f = 0.5$ (i.e., at this value, $1/\tau_M < 0$), a periodic orbit is obtained, as clearly seen in Figs. 6(a) and 6(b). In contrast, for $f = 2.0$ (i.e., at this value, $1/\tau_M > 0$), a chaotic orbit occurs, which is clearly observed in Figs. 6(c) and 6(d). These figures confirm that the analytical results agree well with the numerical results.

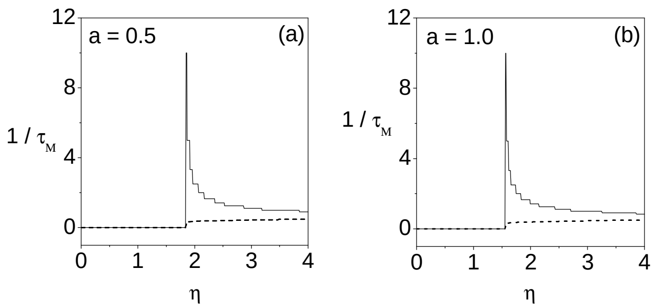

FIGURE 7. Variation of $1/\tau_M^{\pm}$ versus η for two values of $a = 0.5$ and 1.0. Continuous curve is for positive sign of $M(\tau)$ and dashed curve is for negative sign of $M(\tau)$ given by Eq.(3.33). The values of the other parameters in Eq.(3.33) are $f = 0.1, \alpha = 0.8, b = 3.0$ $\Omega = \omega = 2$.

4.1.2. **Horseshoe Chaos for Varying η and Fixed f.** Then, we analyze the occurrence of horseshoe chaos numerically by varying the amplitude η with fixed f. To visually represent the range where horseshoe chaos is possible, we plot in Fig. 7 the dependence of the amplitude η of the parametric forcing for two different values of a, namely, $a = 0.5$ and $a = 1.0$. In Fig. 7(a), for $a = 0.5$, horseshoe chaos does not occur when $\eta < \eta_M = 1.872075$, but horseshoe chaos occurs when $\eta > \eta_M$. In Fig. 7(b), for $a = 1.0$, $1/\eta_{M^\pm}$ is zero when $\eta < \eta_M = 1.503267$, meaning horseshoe chaos is not possible. However, when $\eta > \eta_M = 1.503267$, horseshoe chaos occurs. As the depth of the well increases, the threshold for horseshoe chaos (η_M) decreases, which is clearly evident in Figs. 7(a) and 7(b). From Figs. 3 and 7, we observe that when the depth of the potential well (a) increases, the threshold for horseshoe chaos increases by varying the amplitude (f) of the external excitation. In contrast, the threshold for horseshoe chaos decreases when the depth of the well (a) decreases by varying the amplitude (η) of the parametric excitation. These analytical results are verified numerically.

Figure 8 shows the bifurcation diagrams of the system (Eq. 2.3) as the amplitude (η) of the parametric forcing excitation increases from small values for two fixed values of a, namely, $a = 0.5$ and $a = 1.0$. The other parameters are fixed at $\alpha = 0.8$, $b = 3.0$, $f = 0.1$, and $\omega = \Omega = 2.0$. In Fig. 8(a), for $a = 0.5$, the onset of chaos occurs at $\eta_c = 1.882375$, while for $a = 1.0$, the onset of chaos occurs at $\eta_c = 1.516342$, as clearly seen in Fig. 8(b). From Figs. 7 and 8, the analytical results agree well with

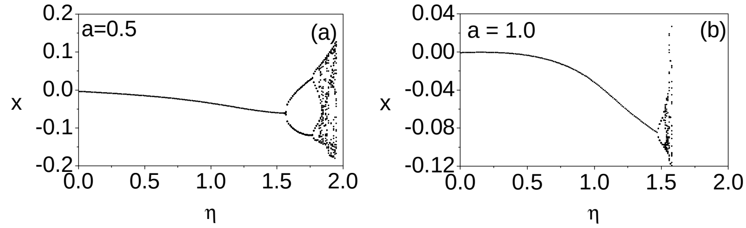

FIGURE 8. Bifurcation diagrams of the system (Eq.2.3) as a function of η for (a) $a = 0.5$ and (b) $a = 1.0$. The values of the other parameters in Eq.(2.3) are $f = 0.1, \alpha = 0.8, b = 3.0, \Omega = \omega = 2.0$.

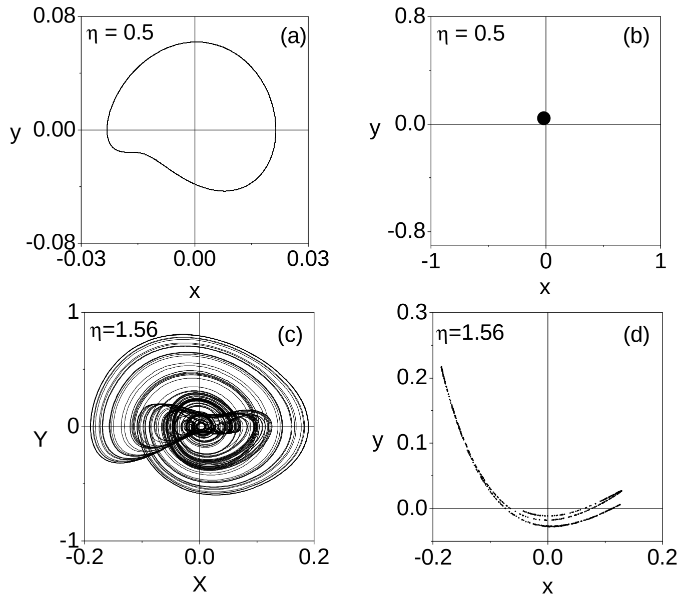

FIGURE 9. Phase portraits and the corresponding Poincaré maps of the system (Eq.2.3) for showing the (a-b) periodic orbit for $\eta = 0.5$ and (c-d) chaotic orbit for $\eta = 1.56$. The values of the other parameters in Eq.(2.3) are $a = 1.0, f = 0.1, \alpha = 0.8, b = 3.0, \Omega = \omega = 2.0$.

the numerical results. The analytical results are also verified by plotting the phase portrait and Poincaré map of the system (Eq. 2.3) for two values of η, chosen from Fig. 7(b). The results are presented in Fig. 9. For $\eta = 0.5$ (i.e., $\eta < \eta_M = 1.503267$), periodic behavior occurs, as shown in Figs. 9(a) and 9(b). For $\eta = 1.56$ (i.e., $\eta > \eta_M$), chaotic behavior occurs, as clearly seen in Figs. 9(c) and 9(d). For both values of a, we observe various dynamical behaviors, including bifurcations of periodic orbits, coexisting attractors, and chaotic orbits in the system (Eq. 2.3).

4.2. **The Effect of Damping Strength** (α) **on Bifurcation Analysis.** First, we analyze the effect of parametric excitation on the bifurcation behaviors of the system (Eq. 2.3). The detailed bifurcation diagrams of η versus x for four different values of damping strength (α) are shown in Fig. 10. The other parameters are fixed at $f = 0.1$, $a = 1.0$, $b = 3.0$, and $\omega = \Omega = 2.0$. When $\alpha = 0.3$, we observe periodic solutions

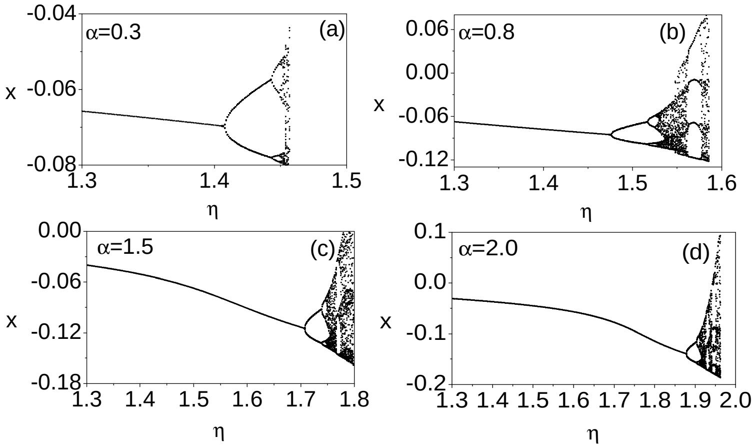

FIGURE 10. Bifurcation diagrams of η versus x for four values of damping strength (α) (a) $\alpha = 0.3$, (b) $\alpha = 1.0$, (c) $\alpha = 1.5$ and (d) $\alpha = 2.0$. The values of the other parameters in Eq.(2.3) are $f = 0.1, a = 1.0, b = 3.0, \Omega = \omega = 2.0$.

with periods $2T$, $4T$, and higher, as well as transient chaotic motion. Finally, at $\eta = 1.45177$, chaotic motion occurs. At $\eta = 1.45782$, the motion becomes unbounded. When the damping strength (α) is increased to 0.8, as seen in Fig. 10(b), chaotic motion occurs later than in Fig. 10(a). Specifically, at $\eta = 1.58718$, the motion becomes unbounded for $\alpha = 0.8$. Further increases in the damping strength (α) lead to the occurrence of chaotic motion later than in Fig. 10(c) and Fig.10(d), with the appearance of a few short periodic windows. For example, for $\alpha = 1.5$ and $\alpha = 2.0$, chaotic motion occurs at $\eta = 1.75302$ and $\eta = 1.91183$, respectively.

Next, we analyze the effect of external excitation on the bifurcation behaviors of the system (Eq. 2.3). The detailed bifurcation diagrams of f versus x for four different values of damping strength (α) are shown in Fig. 11. The other parameters are fixed at $\eta = 0.1$, $a = 1.0$, $b = 3.0$, and $\omega = \Omega = 2.0$. When $\alpha = 0.3$, period-T and period-$2T$ solutions are observed, but no chaotic motion is present (Fig. 11(a)). For $\alpha = 0.8$, 1.5, and 2.0, various bifurcations of periodic orbits, chaotic orbits, and window regions occur, as clearly seen in Figs. 11(b)-(d). As the value of α increases, the onset of chaos is delayed.

4.3. **The Effect of $\omega \neq \Omega$ on Horseshoe Chaos.** In the previous section, we considered the case $\omega = \Omega$. In this section, we study the case $\omega \neq \Omega$ to investigate the occurrence of horseshoe chaos numerically by measuring the time τ_M elapsed between two successive transverse intersections. τ_M can be calculated from Eq. (3.33). Figure 12 shows the plot of $1/\tau_{M^\pm}$ versus f for two values of a. The other parameters are fixed at $\alpha = 0.8$, $b = 3.0$, $\eta = 0.1$, $\omega = 2.0$, and $\Omega = (\sqrt{5}+1)/2$. The continuous curve represents the inverse of the first intersection time $1/\tau_{M^+}$ for the stable and unstable branches of the homoclinic orbits W^+. The dashed curve corresponds to

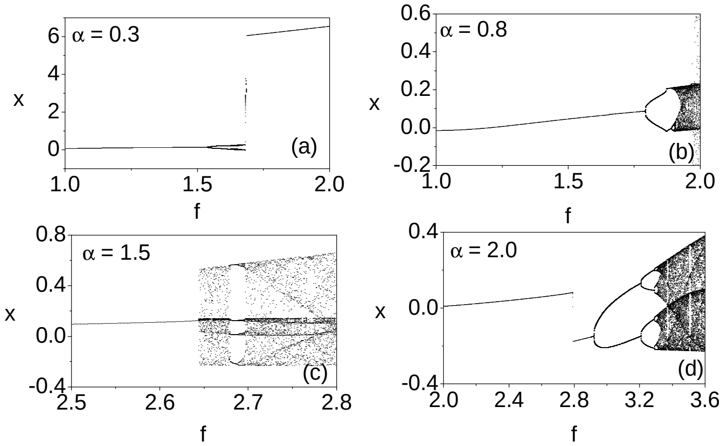

FIGURE 11. Bifurcation diagrams of f versus x for four values of damping strength (α) (a) $\alpha = 0.3$, (b) $\alpha = 1.0$, (c) $\alpha = 1.5$ and (d) $\alpha = 2.0$. The values of the other parameters in Eq.(2.3) are $\eta = 0.1, a = 1.0, b = 3.0, \Omega = \omega = 2.0$.

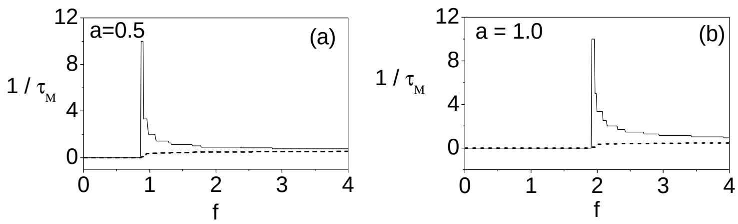

FIGURE 12. Variation of $1/\tau_M^{\pm}$ versus f for two values of $a = 0.5$ and 1.0. Continuous curve is for positive sign of $M(\tau)$ and dashed curve is for negative sign of $M(\tau)$ given by Eq.(3.33). The values of the other parameters in Eq.(2.3) are $\eta = 0.1, \alpha = 0.8, b = 3.0, \Omega = (\sqrt{5} + 1)/2$ and $\omega = 2$.

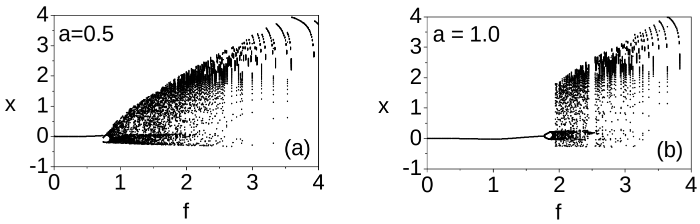

FIGURE 13. Bifurcation diagrams of the system (Eq.2.3) as a function of f for (a) $a = 0.5$ and (b) $a = 1.0$. The values of the other parameters in Eq.(2.3) are $\eta = 0.1, \alpha = 0.8, b = 3.0, \Omega = (\sqrt{5} + 1)/2$ and $\omega = 2.0$.

the orbit of W^-. Horseshoe chaos does not occur when $1/\tau_M$ is zero, and it occurs in the region where $1/\tau_M > 0$. In Fig. 12(a), where the value of a is fixed at 0.5, $1/\tau_{M^+}$ is zero in the interval $0 < f < 0.881075$, and thus no horseshoe chaos occurs in this interval of f. For values of $f > 0.881075$, horseshoe chaos is possible. In Fig. 12(b), where the value of a is fixed at 1.0, $1/\tau_{M^\pm}$ is zero for $0 < f < 1.9750438$, and

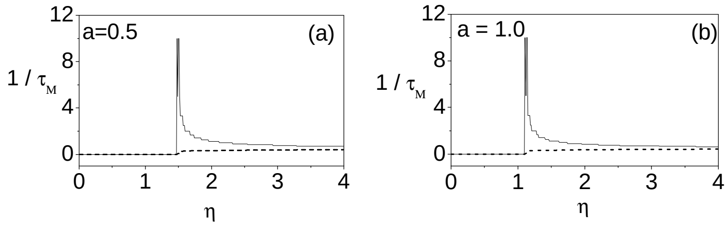

FIGURE 14. Variation of $1/\tau_M^{\pm}$ versus η for two values of $a = 0.5$ and 1.0. Continuous curve is for positive sign of $M(\tau)$ and dashed curve is for negative sign of $M(\tau)$ given by Eq.(3.33). The values of the other parameters in Eq.(2.3) are $f = 0.1, \alpha = 0.8, b = 3.0, \Omega = (\sqrt{5}+1)/2$ and $\omega = 2$.

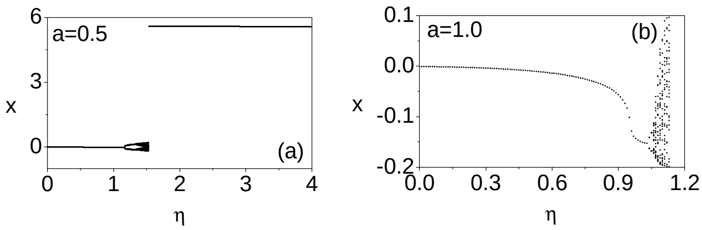

FIGURE 15. Bifurcation diagrams of the system (Eq.2.3) as a function of η for (a) $a = 0.5$ and (b) $a = 1.0$. The values of the other parameters in Eq.(2.3) are $f = 0.1, \alpha = 0.8, b = 3.0, \Omega = (\sqrt{5}+1)/2$ and $\omega = 2.0$.

nonzero for $f > 1.975043$. The analytical results obtained from Fig. 12 are verified by directly integrating the system (Eq. 2.3). The numerical results are presented in Fig. 13. In Figs. 13(a) and 13(b), for $a = 0.5$ and $a = 1.0$, the onset of chaos occurs at $f_c = 0.875189$ and $f_c = 1.983872$, whereas the analytical values are $f_M = 0.881075$ for $a = 0.5$ and $f_M = 1.975043$ for $a = 1.0$. From Figs. 12 and 13, the analytical results agree well with the numerical results.

Similarly, we analyze the occurrence of horseshoe chaos by varying η with a fixed f for the case $\omega \neq \Omega$. The other parameters are fixed at $\alpha = 0.8$, $b = 3.0$, $f = 0.1$, $\omega = 2.0$, and $\Omega = (\sqrt{5}+1)/2$. The analytical and numerical results are presented in Figs. 14 and 15. In Fig. 14, the analytical values for the occurrence of horseshoe chaos are $\eta_M = 1.501292$ for $a = 0.5$ (Fig. 14(a)) and $\eta_M = 1.175435$ for $a = 1.0$ (Fig. 14(b)). The numerical results for the onset of chaos are $\eta_c = 1.508752$ for $a = 0.5$ (Fig. 15(a)) and $\eta_c = 1.174782$ for $a = 1.0$ (Fig. 15(b)). These results clearly confirm that the analytical results agree well with the numerical results.

5. **Conclusions**

In this paper, we investigated the intricate dynamics of a linearly damped Morse oscillator under the influence of both parametric and external excitations. The unperturbed Morse oscillator has a degenerate fixed point at infinity, which is regularized by a McGhee-type transformation. The Melnikov method is then applied to this new set of coordinates in the perturbed system. We derived the analytical criteria for the appearance of chaos in the sense of Smale using the Melnikov method. By applying this method, we have determined critical forcing amplitudes f_M and η_M above which the system may exhibit chaotic behavior. We explored the effects of the depth of the potential well (a) and the amplitudes of both parametric and external excitations on the Melnikov critical values. Our analysis reveals that the Melnikov critical values increase as the depth of the well and the external excitation amplitude (f) increase, while they decrease when the depth of the well and the parametric excitation amplitude (η) increase. The same trends were observed in both the $\omega = \Omega$ and $\omega \neq \Omega$ cases. The analytical results were confirmed by plotting bifurcation diagrams, phase portraits, and Poincar maps, as well as by measuring the time (τ_M) elapsed between successive changes in the sign of $M(\tau)$. The numerical simulations not only support the analytical findings but also reveal new and interesting dynamical behaviors. These complex dynamics appear to arise from the combined influences of the depth of the well, parametric, and external excitations.

It is important to further study the effects of two parametric forces in a linearly damped Morse oscillator using both analytical and numerical techniques. This will be addressed in future work.

REFERENCES

[1] M. Faraday, On a peculiar class of acoustical figures; and on certain forms assumed by groups of particles upon vibrating elastic surfaces, *Philosophical Transactions of the Royal Society of London*, 121: 299-340, 1831,.

[2] F.R.S. Lord Rayleigh, On maintained vibrations, *The London, Edinburgh, and Dublin Philosophical Magazine and Journal of Science*, 15(94): 229-235, 1883.

[3] E. Mathieu, Memoire sur le mouvement vibratoire d'une membrane de fo rme elliptique, *Journal de mathematiques pures et appliquees*, 13: 137-203, 1868.

[4] G.W. Hill, On the part of the motion of the lunar perigee which is a function of the mean motions of the sun and moon, *Acta mathematica*, 8(1): 1-36, 1886.

[5] H. Poincare, *Theorie mathematique de la lumiere. Gauthier Villars*, 1892.

[6] J. Guckenheimar and P. Holmes, *The Nonlinear Oscillations, Dynamical Systems and Bifurcations of Vector Fields*, Springer, New York, 1983.

[7] S. Wiggins, *Introduction to applied nonlinear dynamical systems and chaos*, New York, Heidelberg, Berlin, Springer-Verlag,1980.

[8] R.H. Plaut, J.C. Hsieh, Chaos in a mechanism with time delays under parametric and external excitation, *Journal of Sound and Vibration*, 114(1): 73-90, 1987.

[9] K. Szabelski and J. Warminski, Self-excited system vibrations with parametric and external excitations, *Journal of Sound and Vibration*, 187(4): 595-607, 1995.

[10] P. Chacon, Suppression of chaos by selective resonant parametric perturbation, *Phys. Rew. E*, 51: 761-764, 1995.

[11] C.H. Miwadinou, A.V. Monwanou, A.A. Koukpemedji, Y.J.F. Kpomahou, and J.B. Chabi Orou, Chaotic motions in forced mixed Rayleigh-Lienard oscillator with external and parametric periodic excitations, *International Journal of Bifurcation and Chaos*, 28(3): 1830005-116, 2015. .

[12] V.K. Melnikov, On the stability of a center for time-periodic perturbations, *Trans. Moscow Math. Soc.*, 12: 1-57, 1963. .

[13] I. Mezic and S. Wiggins, On the integrability and perturbation of three-dimensional fluid flows with symmetry, *Journal of Nonlinear Science*, 4(1): 157, 1994.

[14] L. Zhou, S. Liu, and F. Chen, Chaotic dynamics of a Rayleigh-Duffing oscillator with periodically external and parametric excitations, *in Proceedings of the 6th International Conference on Mechatronics, Materials, Biotechnology and Environment*, pp. 286292, Atlantis Press, Yinchuan, China, August 2016.

[15] Y.J.F. Kpomahou and J.A. Adechinan, Nonlinear dynamics and active control in a Lienard-type oscillator under parametric and external excitations, *American Journal of Computational and Applied Mathematics*, 10(2): 4861, 2020.

[16] V. Ravichandran, S. Jeyakumari, V. Chinnathambi, S. Rajasekar and M.A.F. Sanjuan, Role of asymmetries on the chaotic dynamics of Double-well Duffing oscillator, *Pramana -Journal of Physics*, 72: 927-937, 2009.

[17] L. Ravisankar, V. Ravichandran and V. Chinnathambi, Prediction of horseshoe chaos in DVP oscillator driven by different periodic forces, *Int. Journal of Eng. and Sci.*, 1(5): 17-25, 2012.

[18] M.V. Sethu Meenakshi, S. Athisayanathan, V. Chinnathambi, S. Rajasekar, Analytical estimates of the effect of amplitude modulated signal in nonlinearly damped Duffing-vander Pol oscillator, *Chinese Journal of Physics*, 55: 2208-2217, 2017.

[19] M.V. Sethumeenakshi, S. Athisyanathan, V. Chinnathambi and S. Rajasekar, Effect of narrow band Frequency modulated signal on Horseshoe chaos in nonlinearly damped Duffing-vander Pol oscillator, *Annual Review of Chaos, Theory, Bifurcations, and Dynamical Systems*, 7: 41-55, 2017.

[20] M.V. Sethu Meenakshi, S. Athisayanathan, V. Chinnathambi and S. Rajasekar, Homoclinic Bifurcation in a Parametrically Driven Nonlinearly Damped DVP Oscillator, *International Journal of Advances in Applied Mathematics and Mechanics*, 5(4): 10-20, 2018.

[21] S. Valli Priyatharsini, M.V. Sethu Meenakshi, V. Chinnathambi and S. Rajasekar, Horseshoe dynamics in Duffing oscillator with fractional damping and multi−frequency excitation, *Journal of Mathematical Modeling*, 7(3): 263-276, 2019.

[22] V. Ravichandran, V. Chinnathambi and S. Rajasekar, Effect of Rectified and Modulated Sine Forces in Duffing oscillator, *Indian Journal of Physics*, 83: 1593-1603, 2009.

[23] V. Ravichandran, V. Chinnathambi and S. Rajasekar, Homoclinic bifurcation and Chaos in Duffing oscillator driven by an modulated force, *Physica A*, 376: 223-236, 2007.

[24] S. Vallipriyatharsini, A. Zeenath Bazeera, V. Chinnathambi and S. Rajasekar, Homoclinic transition to chaos in the Duffing oscillator driven by periodic piecewise linear forces, *Journal of Nonlinear Analysis & Optimization: Theory & Applications*, 13(1): 25-38, 2022.

[25] P.S. Dardi and S.K. Gray, Classical and quantum mechanical studies of HF in an intense laser field, *J. Chem. Phys.*, 77: 1345-1353, 1982.

[26] F.W. Josellis, Morse Theory for Forced Oscillations of Hamiltonian Systems on $Tn \times Tn$, *J. Differential Equations*, 111: 360-384, 1994. https://doi.org/10.1006/jdeq.1994.1086.

[27] H. Kobessi, M. Kobessi & C.H. Tard, On non-integral E-corrections in perturbation theory: application to the perturbed Morse oscillator, *Can. J. Phys.*, 72: 80-85. 1994.

[28] S. Parthasarathy & M. Lakshmanan, Analytic structure of the damped driven Morse oscillator, *Physics Letters A*, 57(6-7): 365-370, 1991. https://doi.org/10.1016/0375-9601(91)90871-5.

[29] D. Permann & I. Hamilton, Wavelet analysis of time series for the weakly forced and weakly damped Morse oscillator, *J. Chem. Phys.*, 100: 379-386, 1994. https://doi.org/10.1063/1.466951.

[30] M.E. Goggin and P.W. Milonni, Driven Morse oscillator: Classical chaos, quantum theory, and photodissociation, *Phys. Rev. A*, 37(3): 796-806, 1988, doi = 10.1103/PhysRevA.37.796.

[31] B.A. Pettitt, The Morse Oscillator and Second-Order Perturbation Theory, *J. Chem. Educ.*, 75: 1170, 1998. https://doi.org/10.1021/ed075p1170.

[32] J. Wu & J. Cao, Linear and nonlinear response functions of the Morse oscillator: Classical divergence and the uncertainty principle, *J. Chem. Phys.*, 115: 5381-5391, 2001. https://doi.org/10.1063/1.1389840.

[33] U. Leonhardt, State reconstruction of anharmonic molecular vibrations: Morse oscillator model, *Phys. Rev. A*, 55: 3164, 1997. https://doi.org/10.1103/PhysRevA.55.3164.

[34] S. Guruparan, V. Ravichandran , V. Chinnathambi and S. Rajasekar, Coexistence of Multiple attractors , Hysteresis and Vibrational resonance in the classical Morse oscillator driven by an amplitude modulate signal, *Ukraine Journal of Physics*, 62(1): 51-59, 2017.

[35] S. Guruparan, B. Ravindran Durai Nayagam, V. Ravichandran, V. Chinnathambi & S. Rajasekar, Vibrational resonance in the classical Morse oscillator driven by NBFM and WBFM signals, *Journal of Pure Applied Chemical Research*, 5(3): 131-141, 2016.

[36] S. Guruparan, B. Ravindran Durai Naayagam, S. Selvaraj, V. Ravichandran & V. Chinnathambi, Bifurcation structures of the classical Morse oscillator under the excitation of different periodic forces, *Journal of Advanced Chemical Sciences*, 2(1): 188-191, 2016.

[37] K. Abirami, S. Rajasekar & M.A.F. Sanjuan, Vibrational resonance in the Morse oscillator, *PRAMANA J. of Physics*, 81(1): 127141, 2013.

[38] W. Knob & W. Lauterborn, Bifurcation structure of the classical Morse oscillator, *J. Chem. Phys.*, 93: 3950–3957, 1990.

[39] Z. Jing, J. Deng & J. Yang, Bifurcations of periodic orbits of chaos in damped and driven Morse oscillator, *Chaos, Solitons and Fractals*, 35: 486-505, 2008.

[40] D. Beigie & S. Wiggins, Dynamics associated with a quasi-periodically forced Morse oscillator: Application to molecular dissociation, *Phys. Rev. A*, 45: 4803-4827, 1992 .

[41] P. M. Morse, Diatomic molecules according to the wave mechanics. II. Vibrational levels, *Physical Review*, 34(1): 57, 1929.

[42] R. McGehee, A stable manifold theorem for degenerate fixed points with applications to celestial mechanics, J. Differential Equations, 14; 7088, 1973.

[43] B. Bruhn, Homoclinic bifurcations in simple parametrically driven systems, *annalen der physik*, 501(5): 367-375, 1989. https://doi.org/10.1002/andp.19895010506

[44] M. David, *Ph.D thesis, Drysdale Jesus College, University of Oxford*. Michaelmas Term, 1994 ”Homoclinic bifurcations” https://www.lurklurk.org/homoclin.pdf